

# A Five-Planet Resonant Chain: Reevaluation of the Kepler-80 System

MARIAH G. MACDONALD,<sup>1</sup> CODY J. SHAKESPEARE,<sup>1,2</sup> AND DARIN RAGOZZINE<sup>3</sup>

<sup>1</sup>*Department of Astronomy & Astrophysics, Center for Exoplanets and Habitable Worlds, The Pennsylvania State University, University Park, PA 16802, USA*

<sup>2</sup>*Department of Physics and Astronomy, University of Nevada, Las Vegas, 4505 S. Maryland Pkwy, Las Vegas 89154, USA*

<sup>3</sup>*Department of Physics and Astronomy, Brigham Young University, N283 ESC, Provo, UT 84602, USA*

## ABSTRACT

Since the launch of the Kepler space telescope in 2009 and the subsequent K2 mission, hundreds of multi-planet systems have been discovered. The study of such systems, both as individual systems and as a population, leads to a better understanding of planetary formation and evolution. Kepler-80, a K-dwarf hosting six super-Earths, was the first system known to have four planets in a chain of resonances, a repeated geometric configuration. Transiting planets in resonant chains can enable us to estimate not only the planets' orbits and sizes but also their masses. Since the original resonance analysis and TTV fitting of Kepler-80, a new planet has been discovered whose signal likely altered the measured masses of the other planets. Here, we determine masses and orbits for all six planets hosted by Kepler-80 by direct forward photodynamical modeling of the lightcurve of this system. We then explore the resonant behaviour of the system. We find that the four middle planets are in a resonant chain, but that the outermost planet only dynamically interacts in  $\sim 14\%$  of our solutions. We also find that the system and its dynamic behaviour are consistent with *in situ* formation and compare our results to two other resonant chain systems, Kepler-60 and TRAPPIST-1.

**Keywords:** planetary systems; stars: individual (Kepler-80); planets and satellites: dynamical evolution and stability; methods: statistical

## 1. INTRODUCTION

A wealth of knowledge has already been obtained from the Kepler and K2 missions that has revolutionized the field of exoplanets. Subsequent analysis has discovered new classes of planets and systems grandly different from our own Solar System (e.g., Kepler-11, [Lissauer et al. 2011](#)).

Although we are able to constrain planetary radii from the transit method employed by Kepler, much more work is required to recover mass information from the planets with meaningful constraints only possible in a fraction of systems. With estimates of both a planet's size and mass, we are able start exploring its formation history and its composition. A mass estimate requires radial velocity follow-up or for the planets to be gravitationally perturbing each other's orbits enough that we can detect significant variations in the time of transit, or TTVs. Many previous studies have examined TTVs

and successfully derived planets' masses (e.g., [Hadden & Lithwick 2017](#)). Fitting a system's TTVs can lead to determination of the planets' densities and eccentricities, making it one of the best ways to study a system.

One step beyond fitting the system's TTVs requires a self-consistent forward modeling of the system that fits directly to the lightcurve itself. Known as photodynamical modelling, it couples an n-body integrator with a limb-darkened transit model, skipping the requirement of measuring individual transit times ([Ragozzine & Holman 2010](#)). This is particularly valuable in the case of low signal-to-noise transits like we have in Kepler-80. We use the PhotoDynamical Multiplanet Model – PhoDyMM (<https://github.com/dragozzine/PhoDyMM>) – developed by Ragozzine et al., in prep. and used on many past systems. For example, [Mills & Fabrycky \(2017\)](#) fit the lightcurve of Kepler-444 with an early version of PhoDyMM, constraining two planet masses and the orbital elements for all planets.

Kepler-80 is a K-dwarf hosting six super-Earth planets. The two largest planets were first discovered via TTVs by [Xie \(2013\)](#) with orbital periods of 7.05 and

9.52 days. Two more planets were later validated by Lissauer et al. (2014) and Rowe et al. (2014), and the innermost planet Kepler-80f was statistically validated by Morton et al. (2016) with orbital periods of 3.07, 4.64, and 0.99 days, respectively. By fitting the TTVs of the four outer planets<sup>1</sup>, MacDonald et al. (2016) constrained the orbital parameters and the masses of these four planets. They also studied the system’s resonant behaviour, as Kepler-80 was the first exoplanetary system with a confirmed four-body resonant chain.

More recently, Shallue & Vanderburg (2018) used neural nets and discovered a sixth planet with an orbital period of 14.3 days. Although a full analysis of the system’s resonant behaviour was outside the scope of their study, they do recover a period ratio between planets c and g of near 3:2, suggesting that this new planet also participates in the resonant chain confirmed by MacDonald et al. (2016).

By directly forward modeling and fitting the lightcurve of this system with PhoDyMM, we aim to determine the masses and orbits for all six planets hosted by Kepler-80. In addition, we aim to investigate and characterize the resonant behaviour of the five outer planets and explore the formation of the system and its resonant chain.

In Section 2, we discuss our data and our methods. We describe the results of the PhoDyMM fitting in Section 3 and characterize the system’s resonant behaviour in Section 4. We verify that the system and its dynamic behaviour are consistent with *in situ* formation in Section 5. We then discuss our results and compare them to two other resonant systems, TRAPPIST-1 and Kepler-60, before summarizing and concluding in Section 6.

## 2. DATA AND METHODS

### 2.1. Kepler Photometry

We use all photometric data available by Kepler for this study, including 1 minute short cadence observations from Quarters 7, 8, 9, 11, 12, 13, 15, 16, and 17. Kepler-80 fell on Module 3 of the Kepler Space Telescope which suffered a failure early in the mission. Because of this, no data exist for Quarters 6, 7, and 14. The Kepler-80 lightcurve is detrended after masking the six known planets and stitched together following the methods described in Ragozzine et al. in prep.

### 2.2. Photodynamic Fitting

To allow for the estimation of physical and orbital parameters of the small planets in Kepler-80 in a

simultaneous and self-consistent manner, we fit the lightcurve directly instead of the system’s TTVs. We use PhoDyMM which is described in detail in Ragozzine et al., in prep., which we summarize below.

PhoDyMM integrates the Newtonian equations of motion for the star and the six planets. We then use a limb-darkened light-curve model to generate a synthetic lightcurve to compare to our data and measure a log likelihood assuming Gaussian uncertainties from Kepler lightcurve data. We then perform Bayesian parameter inference using Differential Evolution Markov Chain Monte Carlo (DEMC MC, Ter Braak 2006). For each planet, we fit the orbital period  $P$ , the mid-transit time  $t_0$ , the eccentricity  $e$ , the argument of periape  $\omega$ , the sky-plane inclination  $i$ , the longitude of ascending node  $\Omega$ , the radius  $R$ , and the mass  $M$ . In addition, we fit for the star’s mass  $M_\star$  and radius  $R_\star$ , for the two limb-darkening coefficients  $c_1$  and  $c_2$ , and for the amount of dilution from other nearby stars  $d$ .

We employ Gaussian priors on the stellar mass and radius based on values from MacDonald et al. (2016) ( $M = 0.73 \pm 0.03 M_\odot$ ,  $R = 0.678 \pm 0.023 R_\odot$ ). We also fix  $\Omega = 0$  for all planets, given that the system seems to have small mutual inclinations. We employ flat priors on all other parameters, including a flat prior on the square root of the eccentricity. Nearly all parameters are well constrained by the data so we do not explore the effect of different priors.

## 3. RESULTING PLANETARY PARAMETERS

We run a 96-chain DEMC MC with 190,000 steps, saving every 1,000 steps and removing a burn-in of 7,000 steps. To assess long-term stability of our DEMC MC fits, we pull 30 random solutions from the DEMC MC posteriors and numerically integrate them for 100 Myr using REBOUND (Rein & Liu 2012). We find that all 30 solutions are long-term stable. We report the median values and  $1\sigma$  confidence intervals for the results from our photodynamic model in Table 1.

Compared to the masses estimated by MacDonald et al. (2016) ( $6.75^{+0.69}_{-0.51}$ ,  $6.75^{+0.69}_{-0.51}$ ,  $6.75^{+0.69}_{-0.51}$ ,  $6.75^{+0.69}_{-0.51} M_\oplus$ ), our new estimates for the four middle planets of  $5.95^{+0.65}_{-0.60}$ ,  $2.97^{+0.76}_{-0.65}$ ,  $3.50^{+0.63}_{-0.57}$ , and  $3.49^{+0.63}_{-0.57} M_\oplus$  are more precise and smaller, suggesting that the methods we employed in MacDonald et al. (2016) were overestimating the masses. This overestimate, which is most prominent in the outer two planets Kepler-80b and Kepler-80c, may be explained by the additional Kepler-80g that was not modeled in MacDonald et al. (2016). Since Kepler-80f is not dynamically interacting with other planets, we are unable to constrain the planet’s mass. Additionally, we estimate the mass

<sup>1</sup>The inner planet f is not dynamically interacting with the other planets and therefore does not exhibit TTVs

**Table 1.** Resulting Planetary Parameters

Parameter	Kepler-80f	Kepler-80d	Kepler-80e	Kepler-80b	Kepler-80c	Kepler-80g
$P$ (days)	$0.98678^{+0.00001}_{-0.00002}$	$3.0723^{+0.0002}_{-0.0001}$	$4.6447^{+0.0001}_{-0.0002}$	$7.0534 \pm 0.0002$	$9.5231 \pm 0.0001$	$14.651 \pm 0.001$
$R_p$ ( $R_\oplus$ )	$1.031^{+0.033}_{-0.027}$	$1.309^{+0.036}_{-0.032}$	$1.330^{+0.039}_{-0.038}$	$2.367^{+0.055}_{-0.052}$	$2.507^{+0.061}_{-0.058}$	$1.05^{+0.22}_{-0.24}$
$M_p$ ( $M_\oplus$ )	—	$5.95^{+0.65}_{-0.60}$	$2.97^{+0.76}_{-0.65}$	$3.50^{+0.63}_{-0.57}$	$3.49^{+0.63}_{-0.57}$	$0.065^{+0.044}_{-0.038}$
$\rho_p$	—	$14.6^{+1.9}_{-1.7}$	$6.9^{+1.9}_{-1.6}$	$1.45^{+0.33}_{-0.29}$	$1.22^{+0.24}_{-0.21}$	$0.31^{+0.46}_{-0.20}$
$e$	$0.186^{+0.083}_{-0.049}$	$0.0041^{+0.0037}_{-0.0028}$	$0.0035^{+0.0032}_{-0.0024}$	$0.0049^{+0.0036}_{-0.0032}$	$0.0079^{+0.0040}_{-0.0037}$	$0.1303^{+0.0034}_{-0.0037}$
$i$ (deg)	$85.99^{+0.48}_{-0.52}$	$89.24^{+0.46}_{-0.37}$	$88.59^{+0.15}_{-0.16}$	$88.989^{+0.090}_{-0.085}$	$88.744^{+0.049}_{-0.046}$	$88.26^{+0.15}_{-0.07}$
$t_0$ (BJD - 2454900)	$800.33893^{+0.00047}_{-0.00055}$	$795.13111^{+0.00064}_{-0.00067}$	$796.9113 \pm 0.0011$	$758.39386^{+0.00097}_{-0.0011}$	$796.04731^{+0.00049}_{-0.00052}$	$758.5864^{+0.0094}_{-0.0094}$

NOTE—Orbital period  $P$ , planetary radius  $R_p$ , planetary mass  $M_p$ , bulk density  $\rho_p$ , eccentricity  $e$ , sky-plane inclination  $i$ , and mid-transit time  $t_0$  estimates resulting from the photodynamic DEMCMC posteriors. The nominal value for each parameter is the median of the posteriors and the lower and upper uncertainties are the 16th and 84th percentile confidence intervals.

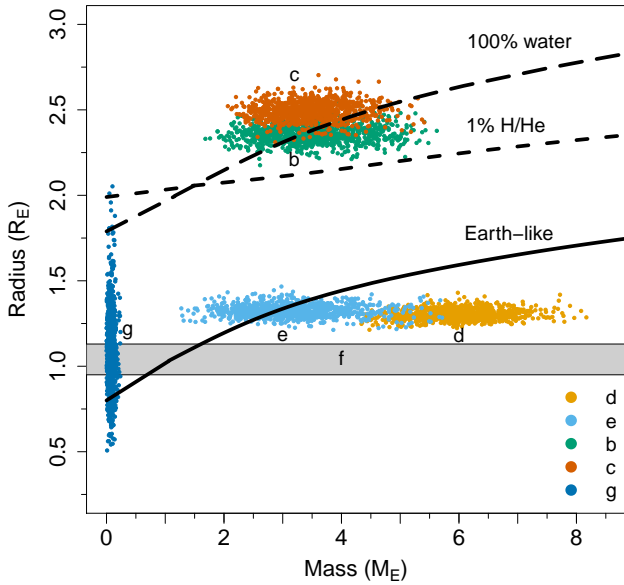


**Figure 1.** Mass-radius diagram with resulting estimates of Kepler-80’s five outer planets. Instead of the typical points and error bars, we pull 200 points from our DEMCMC fitting. Since Kepler-80f is not gravitationally interacting with the other planets, we are unable to constrain its mass and instead plot the  $3\sigma$  range of its radius. Our results are consistent with the measurements from MacDonald et al. (2016) to the  $3\sigma$  level. We estimate smaller masses for the planets, especially for Kepler-80b and Kepler-80c, but estimate similar densities.

of Kepler-80g to be  $0.065^{+0.044}_{-0.038} M_\oplus$  and the radius to be  $1.05^{+0.22}_{-0.24} R_\oplus$ . We show the mass and radius estimates for the five outer planets in Figure 1.

Given the degeneracy between the planets’ masses and eccentricities, MacDonald et al. (2016) limited the eccentricities to less than 0.02. We measure nominal values of 0.0041, 0.0035, 0.0049, 0.0079, and 0.1303 for planets d, e, b, c, and g, respectively, which are consistent

with the measurements from MacDonald et al. (2016) and confirm a dynamically cold system.

Our fits for Kepler-80g suggest that the planet has a fairly small mass ( $\sim 0.6 M_\oplus$ ) for its radius ( $\sim 1.05 R_\oplus$ ), leading to a low bulk density. In addition, we find that the radius of this planet is poorly constrained while the mass appears to be well constrained. We postulate two reasons for this low density and varying precision. First, Kepler-80g has a comparatively low signal-to-noise ratio of 8.6 (Shallue & Vanderburg 2018) compared to the much larger signatures of the other planets in the system (40.4–92.3, MacDonald et al. 2016), which can account for the poor constraint of the planet’s radius. Second, Kepler-80g is most likely not part of the resonant chain (see Section 4), leading to smaller gravitational perturbations with the neighboring planets. These smaller perturbations should lead to the planet’s mass being poorly constrained, but since it is fit with high precision, we conclude that we are most likely over-fitting this planet’s weak signal. Because of these two compounding issues, we caution the reader against drawing conclusions from our measured mass and density of Kepler-80g.

With both radius and mass estimates for our planets, we are able to calculate the planets’ bulk densities and, from here, start to characterize the planets’ compositions. We include composition curves for pure water, Earth-like, and 1% H/He envelopes in our mass-radius diagram (see Figure 1). Like MacDonald et al. (2016), we find that Kepler-80d and Kepler-80e are consistent with an Earth-like composition, although Kepler-80d is likely more dense. Additionally, although we find smaller mass estimates for Kepler-80b and Kepler-80c than MacDonald et al. (2016), we find consistent compositions that require substantial atmospheres of 1–2% H/He. Given the poor constraint on Kepler-80g’s radius, we are unable to constrain the planet’s composi-

tion, although we note it is currently consistent with a terrestrial composition.

Kepler-80d’s density is inferred to be quite high. We model the interiors of Kepler-80d and Kepler-80b using the planet structure code MAGRATHEA (Huang, Rice, and Steffen, in prep.). Here, the core is made of solid and liquid iron, and the mantle is made of perovskite and post-perovskite. To fully explore potential compositions, we model thousands of planets at their nominal masses ( $M_d = 5.95M_\oplus$ ,  $M_b = 3.5M_\oplus$ ) with integer percentages of mass in the planet’s core, mantle, and a water ocean on top of the mantle. For Kepler-80b, we separate our models into suites that include an atmosphere with a mass of 0.0%, 0.01%, and 0.03% of the planet’s mass<sup>2</sup>. We plot the resulting modeled radii as ternary plots in Figure 2 for Kepler-80d and Figure 3 for Kepler-80b. We find that while Kepler-80d must be at least 92% core to satisfy its density, Kepler-80b requires a Venus-like atmosphere ( $\sim 0.01\%$  mass).

Kepler-80 is relatively faint (Kepler magnitude of 14.8), but may be of interest for future observational studies. We draw 100 samples from the posterior distribution and calculate transit times and durations. These are reported in Table 2.

#### 4. FIVE-PLANET RESONANT CHAIN

Kepler-80 earned the title of first exoplanetary system with a confirmed three-body resonant chain of longer than three planets. Before the discovery of the outermost planet g, MacDonald et al. (2016) confirmed and characterized the resonance between the four inner planets d, e, b, and c. These planets are locked in a resonant chain of 4:6:9:12 with two-body resonances between adjacent pairs of 3:2 (e:d), 3:2 (b:e), and 4:3 (c:b). Shallue & Vanderburg (2018) suggest that planet g is included in this chain, bringing the chain to 4:6:9:12:18 with a 3:2 resonance between planets Kepler-80g and Kepler-80c.

These two-body resonances are characterized by the libration of the two-body angles:

$$\Theta_{1-2} = j_1\lambda_1 + j_2\lambda_2 + j_3\omega_1 + j_4\omega_2 + j_5\Omega_1 + j_6\Omega_2, \quad (1)$$

where 1 and 2 refer to two planets,  $\lambda$  is the mean longitude,  $\omega$  is the argument of periaapse,  $\Omega$  is the longitude of ascending node, and the  $j$  coefficients must sum to zero.

In addition to being a set of consecutive two-body angles, a resonant chain can also be characterized by three-body angles, defined as:

$$\phi = p\lambda_1 - (p + q)\lambda_2 + q\lambda_3 \quad (2)$$

where  $\lambda_i$  is the planet’s longitude, planet 1 is the inner planet in the trio, and  $p$  and  $q$  are coefficients describing the resonance.

We pull 1000 fits from our photodynamic model and integrate the systems forward in time to study Kepler-80’s resonant behaviour. We find all three three-body angles, both four-body angles, and the five-body angle to be librating in some of these integrations. We show examples of these librations from one of the fits in Figure 4. In addition, we find that the two-body angles from all adjacent planet pairs rarely librate. We summarize the centers and amplitudes of each of the two- and three-body angles, and the frequency of their libration, in Table 3.

The three-body angles librate about various centers, and the centers of  $\phi_1$  and  $\phi_2$  are strongly correlated. Our bestfit solutions favour libration centers of  $\phi_1 \sim 200^\circ$ ,  $\phi_2 \sim -60^\circ$  (62.8%), while 30.9% result in  $\phi_1 \sim 180.0^\circ$ ,  $\phi_2 \sim 0^\circ$  and the remaining 6.3% of bestfits have angles which librate about  $\phi_1 \sim 162^\circ$ ,  $\phi_2 \sim 55^\circ$ . The primary libration center of  $\phi_1 \sim 200^\circ$  agrees well with both observations (MacDonald et al. 2016) and formation simulations (MacDonald & Dawson 2018). However, the libration center of  $\phi_2 \sim -60^\circ$  does not agree with previous studies ( $\sim -72^\circ$ ). We find no correlations between libration centers and any planetary parameters, but this change in libration center could be due to Kepler-80g, which was unknown at the time of MacDonald & Dawson (2018).

We find that planets d, e, b, and c are always in a resonant chain with the associated three-body angles librating in all of our bestfits. However, Kepler-80g does not always participate in the chain. The three-body angle between planets b, c, and g and the four-body angle between planets e, b, c, and g only librate 8.2% and 14.1% of the time, respectively, and the two-body angle between planets c and g does not librate in any of the bestfits. However, since a resonant chain is defined by all of the planets interacting in the chain with a librating angle, even if not all of the angles librate, Kepler-80 very well could have a five-planet resonant chain.

To explore why the resonant angles are or are not librating, we perform the following analysis. We first look to see if the distributions of planet mass, eccentricity, and argument of periaapse when the outer three-body angle is librating are statistically different than when the angle is not librating using Kolmogorov–Smirnov and

<sup>2</sup>For reference, Venus has an atmospheric mass fraction of  $\sim 0.01\%$



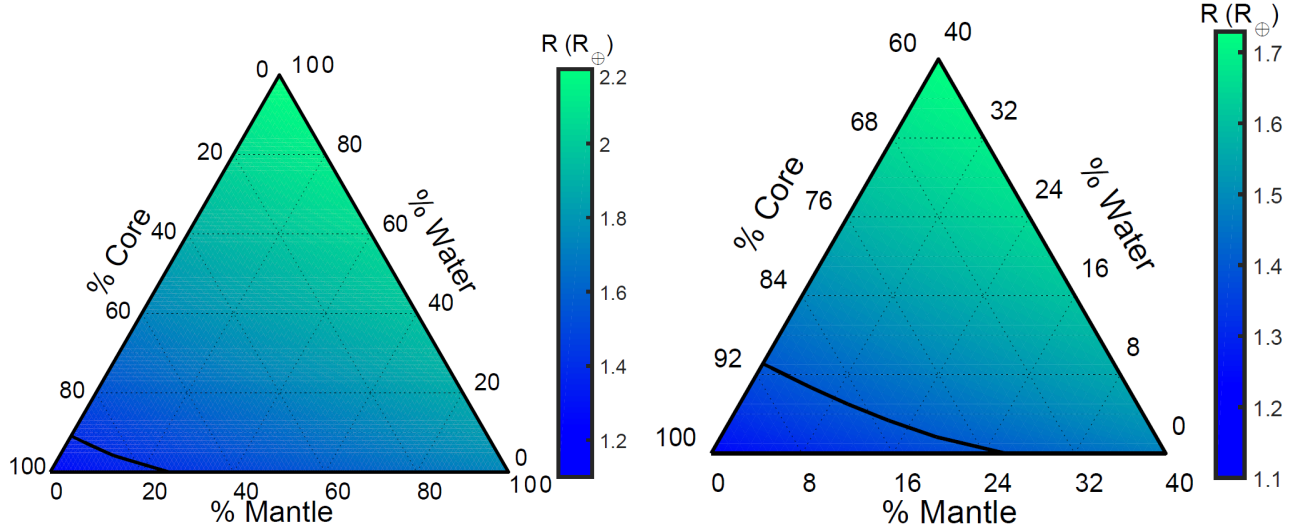


**Figure 2.** left) Ternary diagram from Kepler-80d MAGRATHEA models, where the axes are percentage of mass in a core, mantle, and water ocean. Here, the planet was fixed to a mass of  $5.95M_{\oplus}$ , and the core and mantle are modeled to be pure liquid/solid iron and perovskite and post-perovskite, respectively. We colour the diagram based on the resulting planetary radius, ranging from a minimum radius of  $1.15R_{\oplus}$  to a maximum radius of  $2.2R_{\oplus}$ . We include a contour line for  $R=1.44R_{\oplus}$ , the  $3\sigma$  upper limit of the radius. right) Ternary diagram of the same models, but zoomed in to core mass percentages of 60% – 100%, and therefore with a change in the colourbar scale. We find that Kepler-80d must be at least 92% core to satisfy its density.

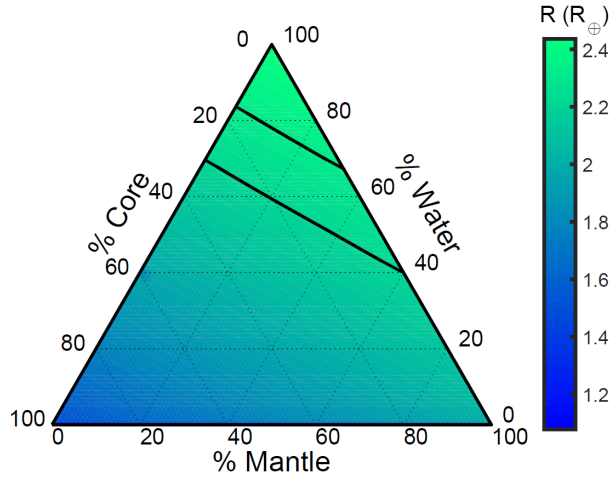


**Figure 3.** Ternary diagram from Kepler-80b MAGRATHEA models, where the axes are percentage of mass in a core, mantle, and water ocean, and we force 0.03% mass into the atmosphere. Here, the planet was fixed to a mass of  $3.5M_{\oplus}$ , and the core and mantle are modeled to be pure liquid/solid iron and perovskite and post-perovskite, respectively. We colour the diagram based on the resulting planetary radius, ranging from a minimum radius of  $1.6R_{\oplus}$  to a maximum radius of  $2.42R_{\oplus}$ . We include contour lines at  $R=2.211R_{\oplus}$  and  $R=2.315R_{\oplus}$ , the  $1\sigma$  and  $3\sigma$  lower limits of the radius. We find that Kepler-80b must contain at least 0.01% mass in its atmosphere to satisfy its low density.

Anderson-Darling two-sample tests. These tests result in large p-values for every planet mass and eccentricity, and so we fail to reject the null hypothesis that the two samples are from the same population.

From both Kolmogorov–Smirnov and Anderson-Darling two-sample tests, we find that Kepler-80e and Kepler-80c have statistically distinct distributions of

their arguments of periaapse when  $\phi_3$  is librating and when it is not librating. This suggests that there is a preferred orientation of the outer planet, most likely because it is eccentric ( $e \sim 0.13$ ).

We then explore Kernel Density Estimates (KDE) of the mass, eccentricity, and argument of periaapse distributions for each planet. We show some of these KDEs

**Table 2.** Future Times and Durations

Planet	Time	$t^+$	$t_-$	Duration	$D^+$	$D_-$
	(BJD-2454900)	min	min	hr	hr	hr
b	4503.90	58.39	-48.99	2.429	0.121	-0.109
b	4510.96	58.44	-49.20	2.429	0.121	-0.109
b	4518.01	59.14	-49.38	2.432	0.125	-0.111
b	4525.07	59.28	-49.27	2.432	0.125	-0.111
b	4532.12	59.53	-49.12	2.430	0.123	-0.109
b	4539.18	59.86	-49.12	2.429	0.121	-0.110
b	4546.23	61.46	-48.19	2.429	0.120	-0.111
b	4553.28	61.90	-48.30	2.429	0.121	-0.110
b	4560.34	62.51	-48.65	2.429	0.121	-0.111
b	4567.39	62.76	-49.65	2.430	0.125	-0.113
b	4574.45	63.66	-49.14	2.427	0.126	-0.112
b	4581.50	63.94	-49.72	2.426	0.122	-0.111
b	4588.55	63.91	-50.12	2.425	0.120	-0.111
b	4595.60	63.84	-50.77	2.425	0.120	-0.111
b	4602.65	63.97	-51.11	2.423	0.120	-0.111

NOTE—Projected future times and durations of transits of the planets in the Kepler-80 system. Times and durations are the 50th percentile, uncertainties are estimated using the 16th and 84th percentiles, mimicking  $1\sigma$  uncertainties. Only a portion of this table is shown here to demonstrate its form and content. A machine-readable version of the full table is available.

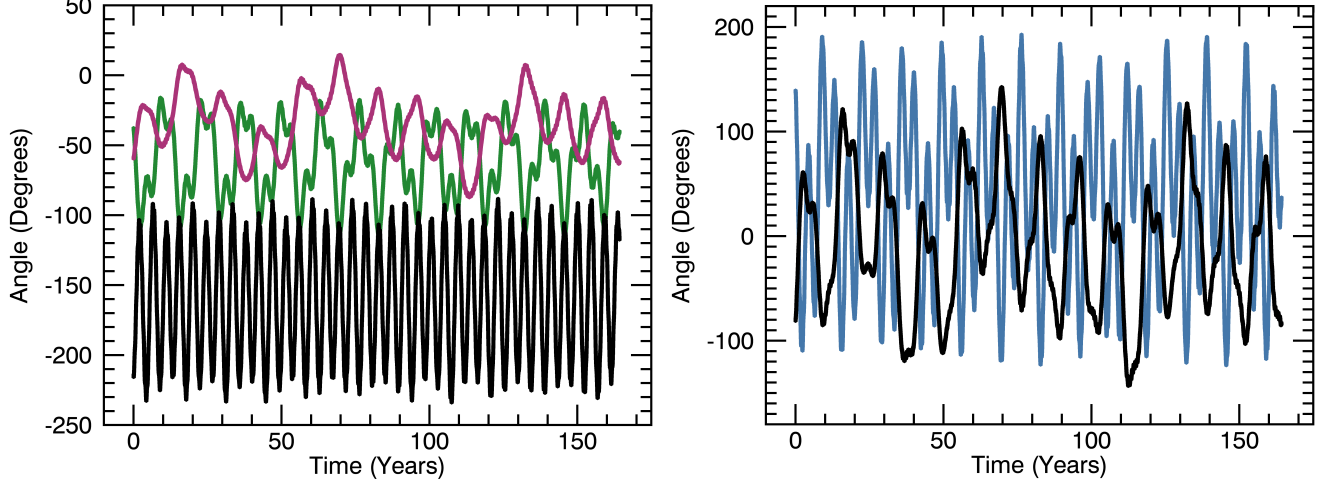


**Figure 4.** Left) Three-body and right) four-body angles from one of the photodynamic fits of Kepler-80. The three-body angles  $\phi_1$ ,  $\phi_2$ , and  $\phi_3$  are colored black, green, and purple, respectively. We plot the inner four-body angle  $\phi_2 - \phi_1$  in blue and the outer four-body angle  $\phi_3 - \phi_2$  as black.

in Figure 5. We find that, within our bestfits, there is a slight preference for a less massive Kepler-80d, a more massive Kepler-80e, and a more massive Kepler-80g for the outer three-body angle  $\phi_3$  to librate. However, we caution against drawing any conclusions from this, as the mass distributions are not statistically distinct. We also find that there is a slight preference for a more ec-

centric Kepler-80d, but again, these two distributions are not statistically distinct. Finally, we find there is a preference for the arguments of periapee of Kepler-80e and Kepler-80c to be  $\sim 150^\circ$  and  $\sim 0^\circ$ , respectively, and the distributions of the angles for these two planets are distinct.

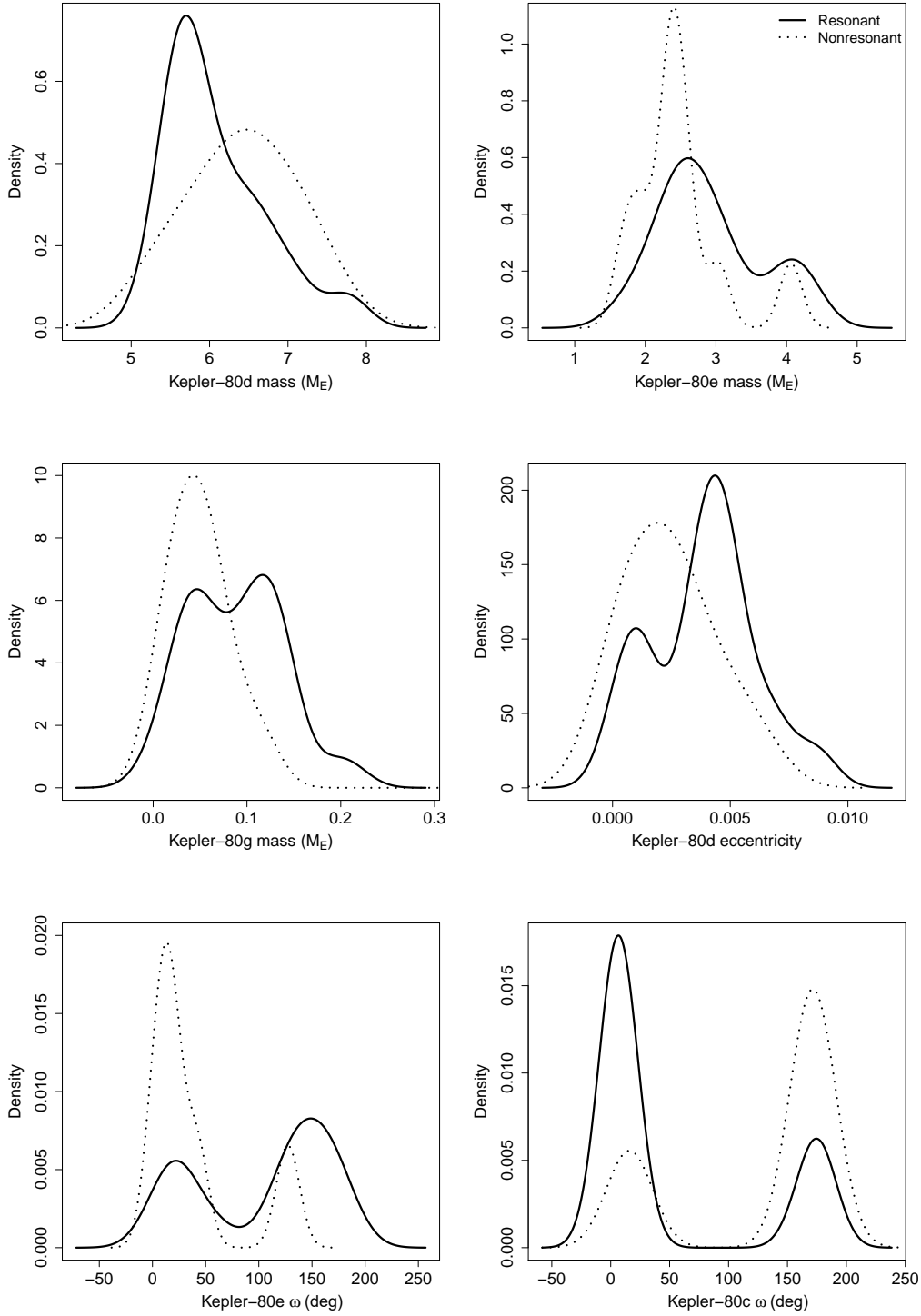


**Figure 5.** Kernel Density Estimates of some mass, eccentricity, and argument of periapse ( $\omega$ ) distributions for each planet, split by whether or not the outer three-body angle  $\phi_3$  was librating. We find that, within our simulations, there is a slight preference for a less massive Kepler-80d, a more massive Kepler-80e, and a more massive Kepler-80g, however, we caution against drawing any conclusions from this, as the mass distributions are not statistically distinct. We also find that there is a slight preference for a more eccentric Kepler-80d, but again, these two distributions are not statistically distinct. Finally, we find there is a preference for the arguments of periapse of Kepler-80e and Kepler-80c to be  $\sim 150^\circ$  and  $\sim 0^\circ$ , respectively. The distributions of the angles for these two planets are distinct, with Anderson-Darling two-sample test p-values of 0.007 and 0.005.

**Table 3.** Resonant Angles

Angle	% libration	Center	Amplitude
$\phi_1 = 3\lambda_b - 5\lambda_e + 2\lambda_d$	100	$200.6 \pm 3.1$ $180.0 \pm 3.9$ $161.9 \pm 4.4$	$39.0 \pm 3.8$ $34.0 \pm 5.5$ $41.1 \pm 4.8$
$\phi_2 = 2\lambda_c - 3\lambda_b + 1\lambda_e$	100	$-60.5 \pm 6.3$ $0.3 \pm 24.3$ $55.0 \pm 9.9$	$16.4 \pm 5.5$ $56.1 \pm 13.7$ $24.3 \pm 5.0$
$\phi_3 = 1\lambda_g - 2\lambda_c + 1\lambda_b$	8.2 46.3 <sup>†</sup>	$-33.8 \pm 42.3$ $166.0 \pm 26.3$	$26.7 \pm 21.2$ $20.5 \pm 15.7$
$\Theta_{d,e} = 3\lambda_e - 2\lambda_d - \bar{\omega}_d$	11.4	$179.9 \pm 0.5$	$32.6 \pm 6.5$
$\Theta_{e,b} = 3\lambda_b - 2\lambda_e - \bar{\omega}_e$	0.1	— *	— *
$\Theta_{b,c} = 3\lambda_c - 2\lambda_b - \bar{\omega}_b$	0	—	—
$\Theta_{c,g} = 3\lambda_g - 2\lambda_c - \bar{\omega}_c$	0	—	—

NOTE—Percentage of librating angles in 1000 randomly sampled DEMCMC bestfits with the associated centers and amplitudes for each resonant angle. We find that the initial chain reported by MacDonald et al. (2016) is always librating. We also find that all five dynamically interacting planets in this system are in a full resonant chain, with every planet in a librating two-, three-, four- or five-body angle, in 14% of our bestfits.

\* This angle librated in one bestfit with a center of 163.5 and an amplitude of 34.4.

## 5. KEPLER-80'S RESONANT CHAIN IS CONSISTENT WITH IN SITU FORMATION

Following MacDonald & Dawson (2018), we explore the formation of the resonant chain of Kepler-80 via in situ formation using  $N$ -body simulations in REBOUND (Rein & Liu 2012). A resonant chain can form in situ via two pathways: with small changes to the planets' semi-major axes (which we will call short-scale migration) and with small changes to the planets' eccentricities (which we will call eccentricity damping). We note that short-scale migration becomes pure eccentricity damping when the semi-major axis damping timescale  $\tau_a$  is large.

We use the same stellar properties as in our photodynamic model ( $M_\star = 0.73M_\odot$  and  $R_\star = 0.68R_\odot$ ) and draw the planetary parameters from our DEMCMC fitting (see Table 1). We do not model Kepler-80f as it is not part of the resonant chain. We start all planets at slightly inflated periods ( $\sim 10\%$ ) and apply a migration force as semi-major axis and eccentricity damping with timescales of  $\tau_a = \log N[10^7, 0.7]$  and  $\tau_e = \log N[10^{4.5}, 1.0]$  using REBOUNDx (Tamayo et al. 2020). We force the planets to migrate for  $5 \times 10^6$  days, before turning off migration and integrating the system for another  $8.6 \times 10^7$  days to verify stability and resonance. We plot the periods, eccentricities, period ratios, and three-body angles of an example simulation where all five outer

planets are part of a resonant chain in Figure 6. We also plot the resonant chain outcome as a function of the two damping timescales  $\tau_a$  and  $\tau_e$  in Figure 7, including simulations from MacDonald & Dawson (2018).

The full resonant chain of Kepler-80 forms under a large range of initial orbital periods (3-15%), planetary masses and inclinations, and damping timescales for both semi-major axis ( $10^6 < \tau_a < 10^9$ ) and eccentricity ( $10^2 < \tau_e < 10^9$ )<sup>3</sup>. We find, then, that Kepler-80 and its five-planet resonant chain are indeed consistent with in situ formation. We note that we cannot yet conclude that this system *definitely* formed in situ, as the data and model parameters are also consistent with long-scale migration (see discussion in MacDonald & Dawson 2018). A further exploration of indicators of in situ vs migration history will be necessary to confirm the formation history of Kepler-80.

### 5.1. No correlation between damping timescales

In exploring the first resonant pair of GJ876, Lee & Peale (2002) fix  $\tau_a$  and set their eccentricity damping timescales to  $\tau_e = \tau_a/K$ , where  $K$  is randomly drawn. Many studies since have forced the damping timescales of the semi-major axis ( $\tau_a$ ) and eccentricity ( $\tau_e$ ) to be derived from one another or correlated (e.g., Tamayo et al. 2017).

However, given the lack of constraint<sup>4</sup> to  $K$  and the growth of computational power in the past few years, these two timescales should be sampled independently from one another. Such an analysis can later lead to interesting discoveries involving how disk and planet properties individually affect planet formation and evolution.

We analyze and expand on the simulations from MacDonald & Dawson (2018) and look to see if specific damping timescales lead to stability and resonance for Kepler-80. These simulations were performed before the discovery of Kepler-80g, and so we only include the four middle planets in our simulations.

We find that there is no correlation between  $\tau_e$  and  $\tau_a$ , aside from a slight slope on the stability boundary at fast semi-major axis damping. Additionally, we find that Kepler-80 almost always forms a full resonant chain, except in a few cases of fast semi-major axis and eccen-

<sup>3</sup>These values result from our simulations as well as those from MacDonald & Dawson (2018).

<sup>4</sup>In many isolated cases,  $\tau_a$  and  $\tau_e$  are correlated, such as in direct tidal damping (e.g., Goldreich & Soter 1966) and tidal torques from a planet embedded in gas (Papaloizou & Larwood 2000), but these derivations are only for one or two planets and typically assume small eccentricities. In addition, this value of  $K$  can be a function of eccentricity, semi-major axis, system age, and/or disk properties.



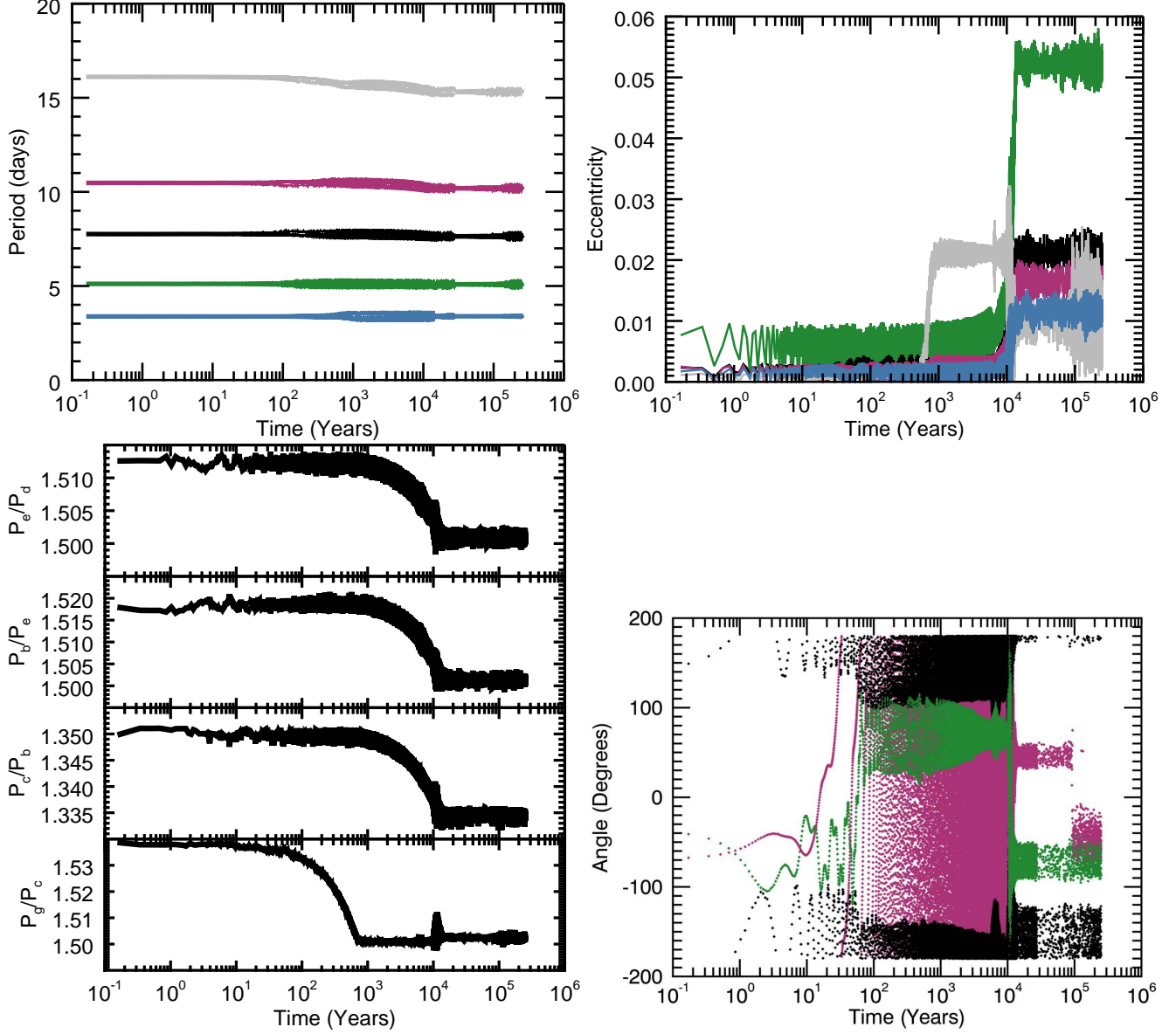


**Figure 6.** Example of a short scale migration simulation where all 5 planets lock into a resonant chain. Here,  $\phi_1 = 3\lambda_b - 5\lambda_e + 2\lambda_d$  (black),  $\phi_2 = 2\lambda_c - 3\lambda_b + 1\lambda_e$  (green), and  $\phi_3 = 1\lambda_g - 2\lambda_c + 1\lambda_b$  (purple). Given that there is a large range of initial conditions that lead to this system being in resonance, we can conclude that this chain is consistent with in situ formation. For this specific example,  $\tau_a = 1.5 \times 10^7$  days and  $\tau_e = 3 \times 10^4$  days, although we explore  $10^6 < \tau_a < 10^9$  days and  $10^2 < \tau_e < 10^9$  days.

tricity damping. Some partial resonant chains also form at slow semi-major axis damping, but these simulations often start with at least one planet pair already in resonance.

We also explore similar parameter spaces for resonant system TRAPPIST-1 and for Kepler-60, a three planet system with a suspected resonant chain. We find that the resonant chain of TRAPPIST-1 can form only under high eccentricity damping ( $\tau_e < 5 \times 10^4$  days), but can form under a range of semi-major axis damping. We

find that most of the simulations, though, result in the system going unstable.

In contrast to TRAPPIST-1, we find that Kepler-60 need not be in a resonant chain to be stable. For a wide range of  $\tau_a$  and  $\tau_e$ , we find that the system is as likely to be non-resonant as it is to have only one resonant pair or to be a fully resonant chain. We plot the results of the short scale migration simulations for all three systems in Figure 7.

Because of the different areas of the  $\tau_a$ - $\tau_e$  parameter space that can result in stability and resonant chain

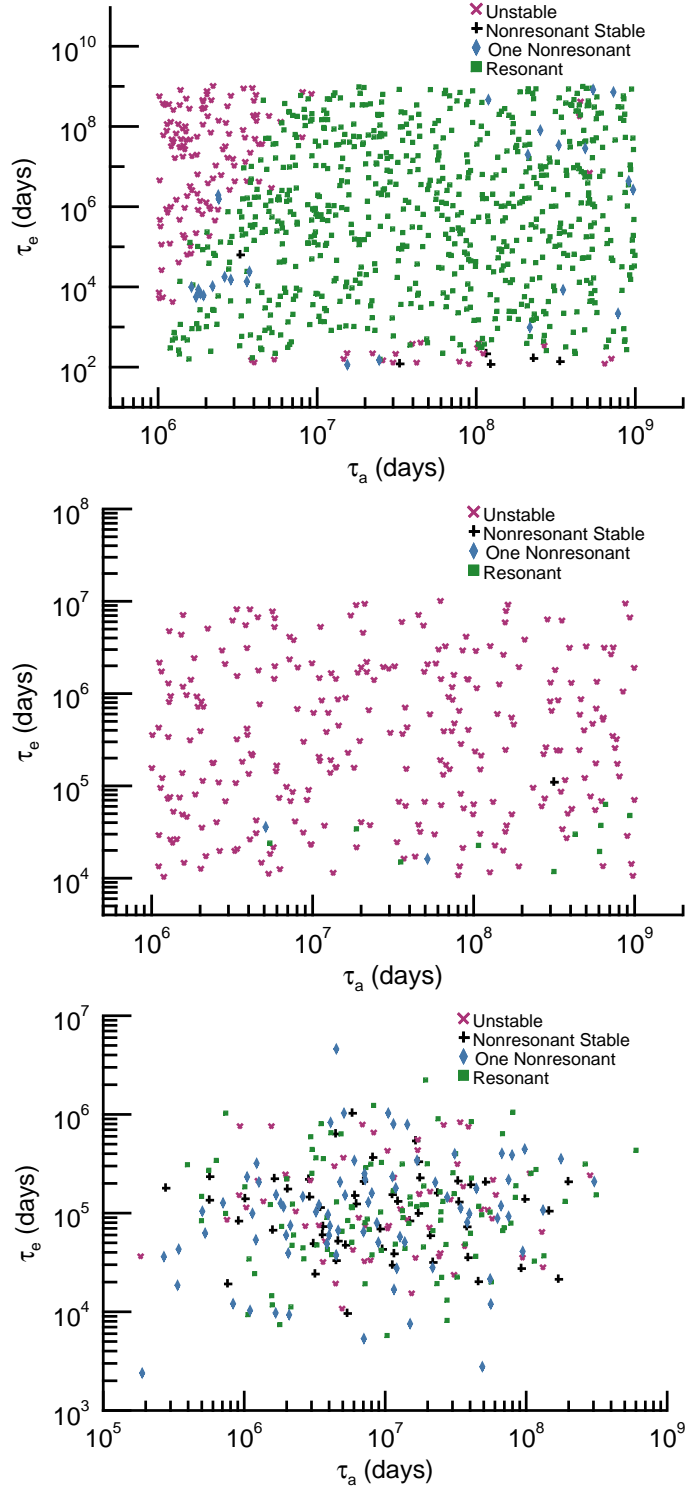


**Figure 7.** Semi-major axis ( $\tau_a$ ) and eccentricity ( $\tau_e$ ) damping timescales for short scale migration simulations from [MacDonald & Dawson \(2018\)](#) and from this work, for top) Kepler-60, middle) TRAPPIST-1, and bottom) Kepler-60. We colour the points based on the outcome of the simulation, where purple x's went unstable, black pluses are stable for the full integration time ( $9.13 \times 10^7$  days) but have more than one planet out of resonance, blue diamonds have one planet not participating in the resonant chain, and green squares have all planets in the resonant chain. Here, we define a resonant chain as each planet interacting with the others via a librating resonant angle, whether that angle is a two-body, and three-body, or a four-body angle. For all three systems, we find no correlation between  $\tau_a$  and  $\tau_e$ . We find that Kepler-80 typically forms a fully librating resonant chain under a wide range of damping timescales. TRAPPIST-1 is long-term stable if it forms its resonant chain, and this is only possible under high eccentricity damping (small  $\tau_e$ ). We find that Kepler-60 does not need to form a resonant chain to remain long-term stable, even after we force short scale migration. Instead, we find that the system is just as likely to be non-resonant as it is to have only two planets in resonance or all planets in resonance.

formation for these three different systems, we caution future studies against forcing a correlation, i.e.,  $\tau_e = \tau_a/K$ . We instead encourage future studies to more fully explore the parameter space for both short-scale and long-scale migration simulations as this can add to the understanding of the initial disk conditions required for the observed system architectures.

## 6. SUMMARY AND CONCLUSION

Recently, [Shallue & Vanderburg \(2018\)](#) used neural nets to uncover another planet in the system Kepler-80, Kepler-80g. This new planet is near the 3:2 period ratio with its neighbor, suggesting that it too is part of the resonant chain confirmed by [MacDonald et al. \(2016\)](#). Given this new planet, we recharacterize the system. We use PhoDyMM to infer orbital and physical parameters for all six planets simultaneously.

We find that, although [MacDonald et al. \(2016\)](#) slightly overestimated the masses of the outer two planets, this was likely due to the signal of then unknown planet g, and our resulting masses are consistent with those from [MacDonald et al. \(2016\)](#) within  $3\sigma$ . We find that Kepler-80c and Kepler-80b require an appreciable atmosphere of  $\sim 1\text{-}2\%$  H/He. Kepler-80d, Kepler-80e, and Kepler-80g are consistent with a terrestrial composition, although Kepler-80d requires has a higher

Fe/Si fraction than Earth, and Kepler-80g may require a small, Venus-like atmosphere.

We next integrate forward 1000 of our bestfits and explore the dynamics of the Kepler-80 system. We find that the three- and four-body resonant angles involving Kepler-80g do not always librate, and the two-body angles for all planet pairs rarely librate. We confirm a four-body resonant chain between planets d, e, b, and c as those associated three-body angles are always librating, but a fully librating five-planet chain only exists in 14% of our bestfit solutions.

Lastly, we explore a potential pathway for the formation of this system and its resonant chain by performing 100  $N$ -body simulations with short scale migration. We find that the chain is consistent with *in situ* formation, although it very well could have formed via other methods.

MGM acknowledges that this material is based upon work supported by the National Science Foundation Graduate Research Fellowship Program under Grant No. DGE1255832. Any opinions, findings, and conclusions or recommendations expressed in this material are those of the author and do not necessarily reflect the views of the National Science Foundation. DR acknowledges the support of Sean Mills and Daniel C. Fabrycky in developing PhoDyMM.

## REFERENCES

- Goldreich, P., & Soter, S. 1966, *icarus*, 5, 375
- Hadden, S., & Lithwick, Y. 2017, *The Astronomical Journal*, 154, 5
- Lee, M. H., & Peale, S. J. 2002, *The Astrophysical Journal*, 567, 596
- Lissauer, J. J., Ragozzine, D., Fabrycky, D. C., et al. 2011, *ApJS*, 197, 8
- Lissauer, J. J., Marcy, G. W., Bryson, S. T., et al. 2014, *ApJ*, 784, 44
- MacDonald, M. G., & Dawson, R. I. 2018, *The Astronomical Journal*, 156, 228
- MacDonald, M. G., Ragozzine, D., Fabrycky, D. C., et al. 2016, *AJ*, 152, 105
- Mills, S. M., & Fabrycky, D. C. 2017, *ApJL*, 838, L11
- Morton, T. D., Bryson, S. T., Coughlin, J. L., et al. 2016, *ApJ*, 822, 86
- Papaloizou, J. C., & Larwood, J. D. 2000, *Monthly Notices of the Royal Astronomical Society*, 315, 823
- Ragozzine, D., & Holman, M. J. 2010, *ArXiv e-prints*, arXiv:1006.3727
- Rein, H., & Liu, S.-F. 2012, *Astronomy & Astrophysics*, 537, A128
- Rowe, J. F., Bryson, S. T., Marcy, G. W., et al. 2014, *ApJ*, 784, 45
- Shallue, C. J., & Vanderburg, A. 2018, *AJ*, 155, 94
- Tamayo, D., Rein, H., Petrovich, C., & Murray, N. 2017, *The Astrophysical Journal Letters*, 840, L19
- Tamayo, D., Rein, H., Shi, P., & Hernandez, D. M. 2020, *Monthly Notices of the Royal Astronomical Society*, 491, 2885
- Ter Braak, C. J. F. 2006, *Statistics and Computing*, 16, 239
- Xie, J.-W. 2013, *ApJS*, 208, 22